

## Influence of Alloy Microstructure on Oxide Growth in HCM12A in Supercritical Water

Jeremy Bischoff<sup>1</sup>, Arthur T. Motta<sup>1</sup>, Lizhen Tan<sup>2</sup> and Todd R. Allen<sup>2</sup>

<sup>1</sup> Department of Mechanical and Nuclear Engineering, Pennsylvania State University, 227 Reber Building, University Park, PA, 16802, USA.

<sup>2</sup> Department of Engineering Physics, University of Wisconsin-Madison, 1500 Engineering Drive, Madison, WI 53706, USA.

### ABSTRACT

HCM12A is a ferritic-martensitic steel alloy envisioned for cladding and structural material in the Generation IV Supercritical Water Reactor (SCWR). This alloy was oxidized in 600°C supercritical water for 2, 4 and 6 weeks, and the oxide layers formed were analyzed using microbeam synchrotron radiation and electron microscopy. The oxide layers show a three-layer structure with an Fe<sub>3</sub>O<sub>4</sub> outer layer, an inner layer containing a mixture of Fe<sub>3</sub>O<sub>4</sub> and FeCr<sub>2</sub>O<sub>4</sub> and a diffusion layer containing FeCr<sub>2</sub>O<sub>4</sub> and Cr<sub>2</sub>O<sub>3</sub> precipitates along ferrite lath boundaries. The base metal microstructure has a strong influence on the advancement of the oxide layers, due to the segregation at the lath boundaries of chromium rich particles, which are oxidized preferentially.

### INTRODUCTION

The Supercritical Water Reactor is one of the six Generation IV nuclear power plant designs and was envisioned for its high thermal efficiency and simplified core [1]. This reactor is designed to function at high outlet temperature (between 500°C and 600°C), which requires cladding and structural materials with good corrosion resistance. Because of their radiation and stress corrosion cracking resistance, ferritic-martensitic steels, such as HCM12A, are candidates for the supercritical water reactor [2].

The oxide layers formed on HCM12A exposed to supercritical water have been previously studied using scanning electron microscopy (SEM), X-ray diffraction (XRD), and electron backscatter diffraction (EBSD) [2-4]. These studies have shown that HCM12A forms a dual layer structure at 500°C with Fe<sub>3</sub>O<sub>4</sub> in the outer layer and spinel (Fe,Cr)<sub>3</sub>O<sub>4</sub> in the inner layer with some evidence of Cr<sub>2</sub>O<sub>3</sub> [4]. At 600°C an internal oxidation layer or diffusion layer is also observed, showing evidence of FeO [2]. The implantation of an yttrium coating prior to oxidation appears to enhance the corrosion resistance of the alloy [2].

In the present study, HCM12A samples were exposed to 600°C SCW for three different exposure times: 2, 4 and 6 weeks. The 4-week sample was implanted with an yttrium surface coating prior to oxidation to investigate the influence of this coating on the corrosion resistance but these results are not shown in this article. The oxide layers formed on HCM12A samples were characterized using scanning and transmission electron microscopy (SEM and TEM), and microbeam synchrotron radiation diffraction and fluorescence. The focus is on determining the phases during the formation and evolution of the oxide layer and to understand the influence of the ferritic-martensitic lath structure of the base metal on the advancement of the oxide layer.

## EXPERIMENTAL PROCEDURES

HCM12A is a ferritic-martensitic steel alloy containing about 10 wt% of chromium. The alloy composition is given in Table 1. The samples studied were normalized at 1050°C for 1 hour then air-cooled before being tempered at 770°C for 7 hours and air-cooled.

**Table I.** Elemental composition of HCM12A in wt%

| Alloy  | C   | N    | Al   | Si  | P    | S    | V   | Cr    | Mn  | Fe   | Ni  | Cu   | Nb   | Mo | W    | Others      |
|--------|-----|------|------|-----|------|------|-----|-------|-----|------|-----|------|------|----|------|-------------|
| HCM12A | .11 | .063 | .001 | .27 | .016 | .002 | .19 | 10.83 | .64 | Bal. | .39 | 1.02 | .054 | .3 | 1.89 | B:<br>31ppm |

The corrosion experiments were performed in the supercritical water corrosion loop at the University of Wisconsin. The supercritical loop is described in more detail in other articles [5, 6]. The pressure used was 25 MPa, the temperature was 600°C and the dissolved oxygen content was ~25ppb. Three exposure times were used: 2, 4 and 6 weeks.

The sample preparation for transmission electron microscopy (TEM) and for microbeam synchrotron radiation is described in detail in previous articles [7-9]. Briefly, 3 mm cross-sectional disk samples were prepared to mirror polish for all the analyses. The TEM samples were prepared from these 3 mm disks using focused ion beam (FIB) (FEI Company Quanta 200 3D Dual Beam FIB) as described previously [10]. The samples were examined in a Phillips 420 at 120 keV, and the electron energy loss spectroscopy (EELS) maps were obtained using a LaB<sub>6</sub> Jeol 2010 at 200 keV. The oxide layers were examined in cross section using diffraction and fluorescence using a 0.2 micron beam at the Advanced Photon Source as done previously [7-9].

## RESULTS AND DISCUSSION

### Characterization of the oxide layers:

Figure 1 shows SEM images and fluorescence spectra of the HCM12A samples oxidized at 600°C for 2, 4 and 6 weeks. The yttrium coating is observed as the white line in the outer layer. The oxide layers formed on HCM12A are similar to the ones observed for other candidate ferritic-martensitic alloys. The SEM images show that in 600°C SCW HCM12A forms a three-layer structure including a non-uniform diffusion layer. The porosity increases in the outer layer and decreases in the inner layer with increasing exposure time. Additionally, oxides form preferentially at lath boundaries in the diffusion layer, which suggests that the oxide advancement is strongly influenced by the base metal microstructure since. The fluorescence data show that the inner layer is enriched in chromium and that the outer layer contains no chromium. Local chromium enrichments are observed at the inner layer-metal interface in the 4-week sample and at the diffusion layer-metal interface (about 16 μm from the outer-inner layer interface) for the 2-week sample. In both cases the associated diffraction data shows peaks consistent with the presence of Cr<sub>2</sub>O<sub>3</sub>. Figure 2 shows an example of the diffraction data collected using microbeam synchrotron radiation diffraction for the 2-week sample.

The diffraction peaks most often observed in the oxide layer can be indexed as Fe<sub>3</sub>O<sub>4</sub> or FeCr<sub>2</sub>O<sub>4</sub>. Although their structures are quite similar, the angular resolution of the microbeam synchrotron radiation diffraction enables us to differentiate between these two oxides [8]. The outer layer contains only Fe<sub>3</sub>O<sub>4</sub>, which is consistent with the absence of chromium in that layer observed in the fluorescence data. On the other hand, the diffusion layer contains a mixture of bcc iron, FeCr<sub>2</sub>O<sub>4</sub> and Cr<sub>2</sub>O<sub>3</sub> and the inner layer contains a mixture of Fe<sub>3</sub>O<sub>4</sub> and FeCr<sub>2</sub>O<sub>4</sub>. A

strong diffraction peak which could be associated with FeO is observed at the inner-diffusion layer interface as seen in other studies [2]. This peak disappears in the 4- and 6-week samples, which suggests that this phase is an intermediate or transient phase in the oxidation process as also observed previously in other alloys [9]. Additionally, base metal grains appear to be present all the way into the inner layer as suggested by the presence of peaks associated with iron bcc.

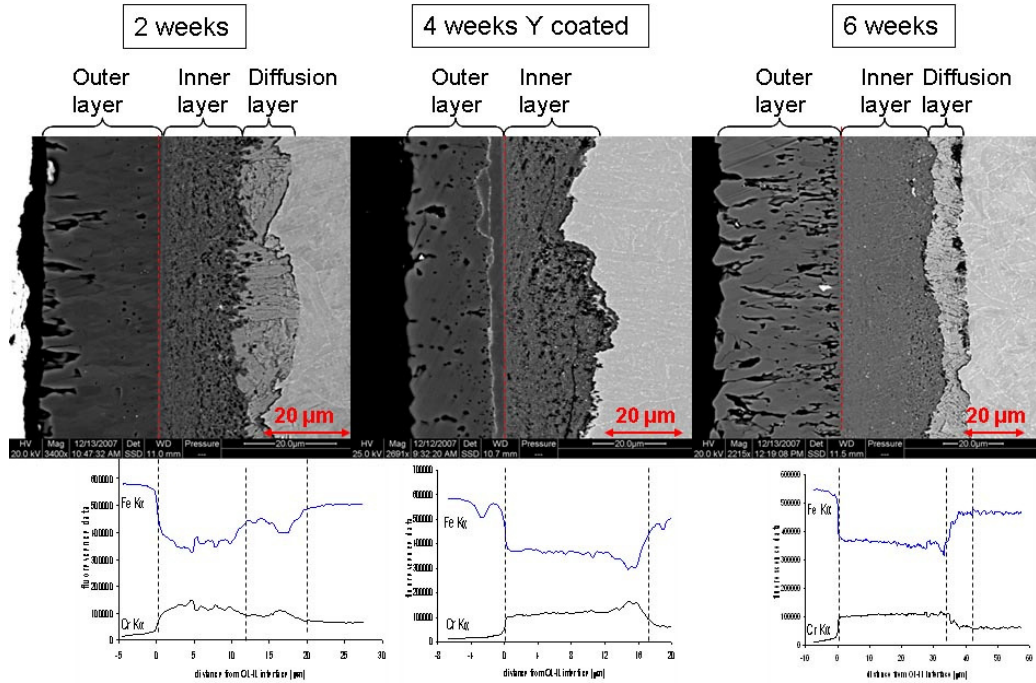


**Figure 1.** SEM images and fluorescence data of the oxide layers formed on HCM12A for 2, 4, and 6 weeks. The 4-week sample was coated with a thin layer of yttrium by sputtering deposition prior to oxidation.

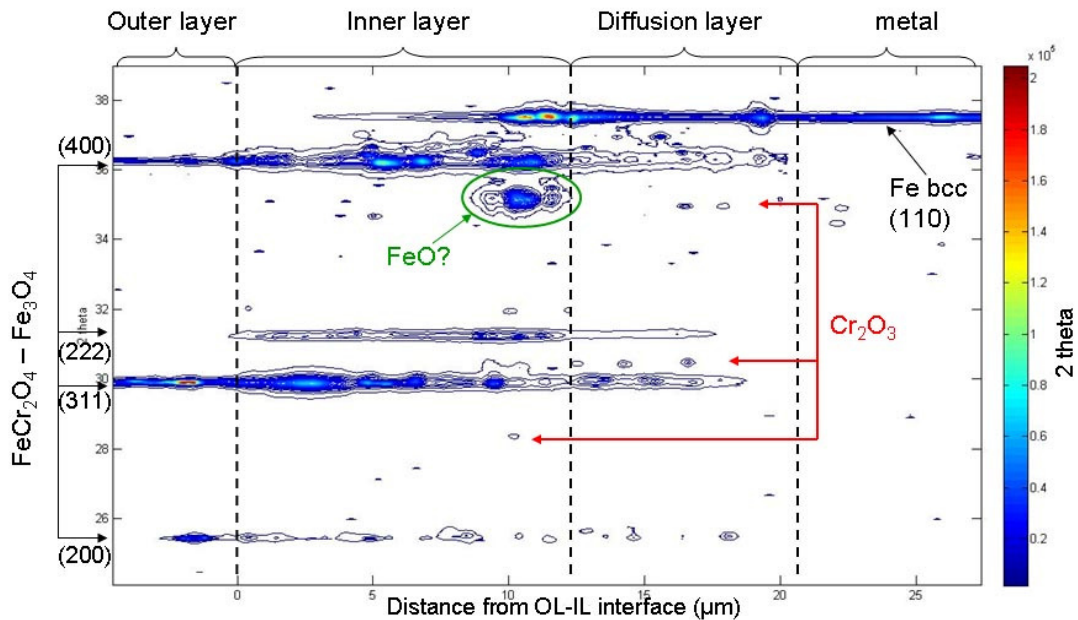


**Figure 2.** Contour plot of the HCM12A 600°C 2-week sample showing the diffraction intensity as a function of the diffraction angle  $2\theta$  and the distance from the outer-inner layer interface in micrometers.

### **Influence of the metal microstructure on oxide growth:**

The influence of the metal microstructure on the oxide growth is most visible in the diffusion layer where oxide precipitates are seen at the lath boundaries along the lines formed by the white spots in the SEM images. Figure 3 shows close-up SEM images of the diffusion layer of the 2-week and the 4-week with the yttrium coating. The dark streaks (arrowed) indicate the oxide formation at the lath boundaries. These boundaries correspond well to those seen in the base metal, which are outlined by particles that appear white in the SEM images.

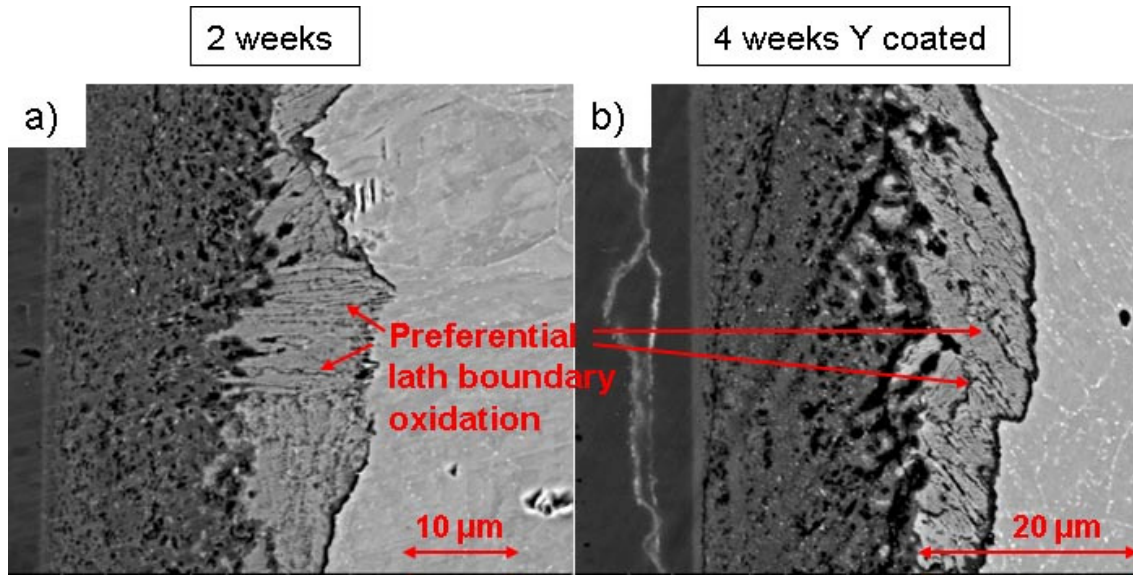


**Figure 3.** SEM images of the diffusion layer of the 2-week (a) and 4-week (b) with yttrium coating samples showing the oxide precipitation along the metal lath boundaries.

The SEM images of Figure 3 clearly show that the base metal microstructure strongly influences the oxide advancement, not only in the diffusion layer but also at the inner-diffusion layer interface. The inner layer advances into the diffusion layer preferentially along the lath boundaries, oxidizing preferentially the chromium rich particles as shown by TEM analysis. A more detailed study of the diffusion layer of the 2-week sample was performed using TEM and especially energy filtered TEM using electron energy loss spectroscopy (EFTEM-EELS). Figure 4 shows a low magnification image and a close-up of the focused ion beam (FIB) TEM sample showing iron, chromium, and oxygen maps. The low magnification images show the lath boundary oxidation in the diffusion layer. The iron and oxygen/chromium maps are indeed complementary to each other indicating the oxides formed are depleted in iron, and rich in chromium and oxygen. The close-up analysis of the oxides shows that, in the lath boundary oxides, chromium and carbon are enriched in the form of lumps. This suggests that, along the lath boundaries, the chromium carbides present at the grain boundaries have been oxidized as chromium rich oxides.

A TEM sample of the base metal from the HCM12A 600°C 2-week sample was prepared using the FIB to identify the particles that formed at the lath boundaries. Figure 5 shows TEM bright field images of an area where three grain boundaries meet and a close-up of a grain boundary showing the particles formed. The TEM bright field images of Figure 5 demonstrate that small particles have formed all along the grain and lath boundaries. The mean particle size is about 200 nm long but can be smaller than 100 nm and larger than 400 nm. The EFTEM-EELS

maps of Figure 5 confirm that the lath and grain boundary region is depleted in iron. The majority of the particles observed at these boundaries appear to be chromium rich. The lath and grain boundaries are also enriched in carbon but not all the chromium particles contain carbon. These results suggest that the oxide front initially advances into the metal by preferential oxidation of chromium carbides at the grain boundary, which allows the formation of the thermodynamically stable chromium oxides.

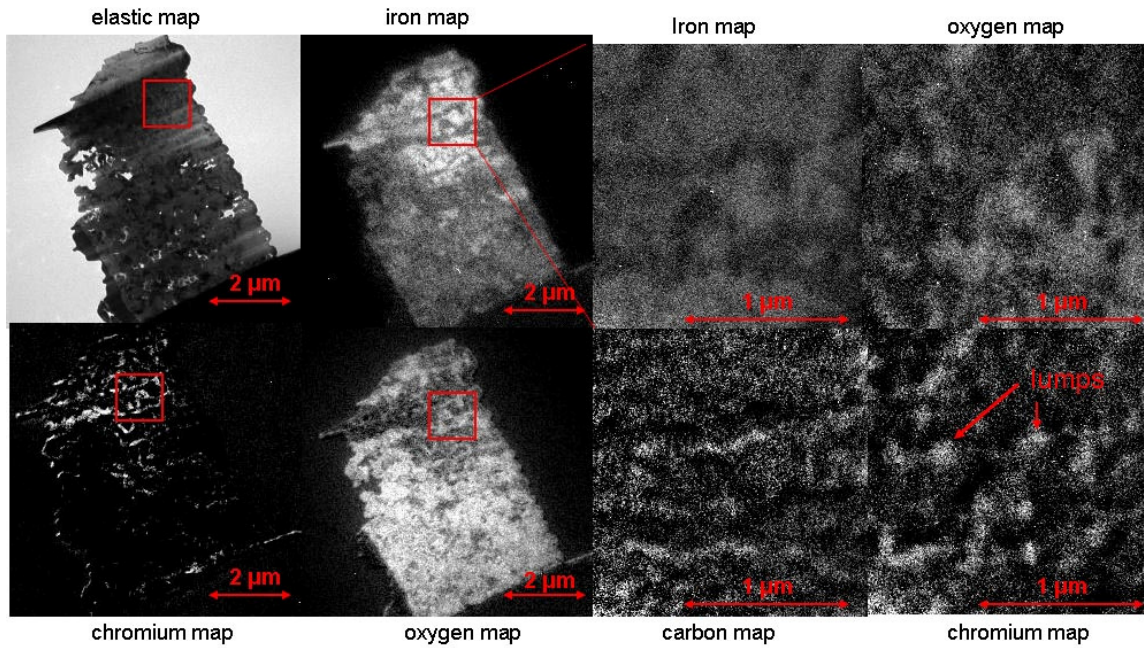


**Figure 4.** EFTEM-EELS energy filtered elemental maps of the inner and diffusion layer of HCM12A 600°C 2 weeks. The set of images on the right are close-up from the region outlined by the red square.

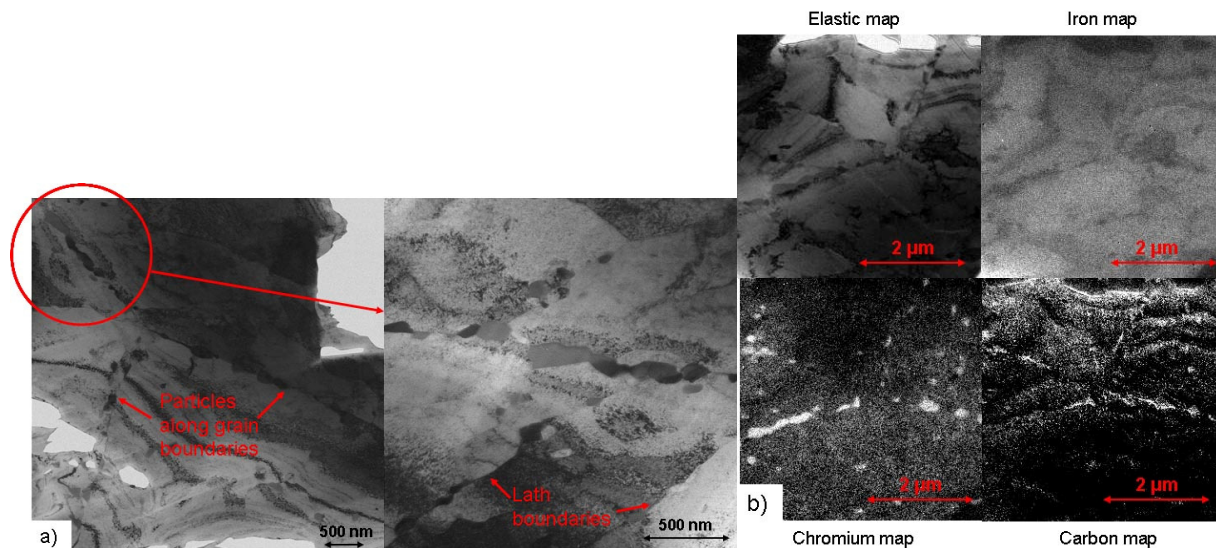


**Figure 5.** a): TEM bright field images of the base metal of HCM12A 600°C 2 weeks. Particles are observed along the grain and lath boundaries. b): EFTEM-EELS maps of the same sample for iron, chromium, and carbon of the particles observed at the lath boundaries.

## CONCLUSIONS

Oxide layers formed on HCM12A during exposure to 600°C supercritical water for 2, 4 and 6 weeks were characterized using electron microscopy and microbeam synchrotron radiation. The main conclusions are:

1. The oxides form a three-layer structure: an Fe<sub>3</sub>O<sub>4</sub> outer layer, an inner layer containing a mixture of FeCr<sub>2</sub>O<sub>4</sub> and Fe<sub>3</sub>O<sub>4</sub>, and a diffusion layer containing FeCr<sub>2</sub>O<sub>4</sub> and Cr<sub>2</sub>O<sub>3</sub> precipitates along iron bcc lath boundaries.
2. Oxide advancement occurs by preferential oxidation of the chromium rich particles, likely carbides, present at the lath boundaries of the base metal.
3. The results suggest that corrosion resistance of the alloy can be modified by changing the base metal microstructure. Therefore engineering methods could be used to enhance corrosion resistance.

## ACKNOWLEDGMENTS

The authors would like to thank Zhonghou Cai and Barry Lai for their help acquiring the data at the APS facility in Argonne National Laboratory. This study is a DOE-NERI funded project (DE-FC07-06ID14744) and the use of the APS was supported by the DOE, Basic Energy Sciences, Office of Science under Contract No. W-31-109-Eng-38. The authors also thank Andrew Siwy and Jamie Kunkle for their assistance and useful discussions during this project.

## REFERENCES

- [1] "A Technology Roadmap for Generation IV Nuclear Energy Systems," U.S. DOE NERAC and Generation IV International Forum GIF-002-00, 2002.
- [2] L. Tan, M. T. Machut, K. Sridharan, and T. R. Allen, *J. of Nucl. Materials*, 371, (2007), 161-170.
- [3] L. Tan, Y. Yang, and T. R. Allen, *Corrosion Science*, 48, (2006), 4234-4242.
- [4] L. Tan, Y. Yang, and T. R. Allen, *Corrosion Science*, 48, (2006), 3123-3138.
- [5] K. Sridharan, S. P. Harrington, A. K. Johnson, J. R. Licht, M. H. Anderson, and T. R. Allen, *Materials & Design*, 28, (2007), 1177-1185.
- [6] K. Sridharan, A. Zillmer, J. R. Licht, T. R. Allen, M. H. Anderson, and L. Tan, "Corrosion Behavior of Candidate Alloys for Supercritical Water Reactors," *Proceedings of ICAPP 04*, Pittsburgh, PA, (2004).
- [7] A. Yilmazbayhan, A. T. Motta, R. J. Comstock, G. P. Sabol, B. Lai, and Z. Cai, *Journal of Nuclear Materials*, 324, (2004), 6-22.
- [8] A. T. Motta, A. D. Siwy, J. M. Kunkle, J. B. Bischoff, R. J. Comstock, Y. Chen, and T. R. Allen, "Microbeam Synchrotron Radiation Diffraction and Fluorescence Study of Oxide Layers formed on 9CrODS Steel in Supercritical Water," *Proceedings of 13th Environmental Degradation of Materials in Nuclear Power Plants*, (2007).
- [9] J. Bischoff, A. T. Motta, and R. J. Comstock, *J. of Nucl. Materials*, in press, accepted manuscript (2009).
- [10] A. D. Siwy, T. E. Clark, and A. T. Motta, *J. of Nucl. Materials*, in press, accepted manuscript (2009).